Source characteristics and along-strike variations of shallow very low frequency earthquake swarms on the Nankai Trough shallow plate boundary

Shunsuke TAKEMURA[1], Satoru BABA[1], Suguru YABE[2], Kentaro EMOTO[3], Katsuhiko SHIOMI[4], and Takanori MATSUZAWA[4]

[1]Earthquake Research Institute, the University of Tokyo, 1-1-1 Yayoi, Bunkyo-ku, Tokyo 113-0032, Japan

[2]Geological Survey of Japan, National Institute of Advanced Industrial Science and Technology, Tsukuba Central 7, 1-1-1 Higashi, Tsukuba, Ibaraki 305-8567, Japan

[3]Geophysics, Graduate School of Science, Tohoku University, 6-3, Aramaki-aza-aoba, Aoba-ku, Sendai 980-8578, Japan

[4]National Research Institute for Earth Science and Disaster Resilience, 3-1 Tennodai, Tsukuba, Ibaraki 305-0006, Japan

Corresponding author: Shunsuke TAKEMURA (shunsuke@eri.u-tokyo.ac.jp)

Key Points:

- Comprehensive detection and source parameter estimations of shallow very low frequency earthquake swarms along the Nankai Trough.

- The scaling relationship between the activity areas and cumulative moments of the swarms roughly follows $Mo \propto A^{3/2}$.

- Along-strike variations of the scaling law for swarm durations reflect differences in the faulting conditions of slow earthquakes.

24 **Abstract**

25 We detected shallow very low frequency earthquakes (VLFEs) off the Cape Muroto and Kii
26 Channel in the Nankai subduction zone and estimated their moment rate functions. Combining
27 the new and previously estimated catalogs, we obtained the comprehensive catalog of shallow
28 VLFE moment rate functions along the Nankai Trough. We defined the shallow VLFE swarms
29 and investigated the scaling relationships of their cumulative moments, activity area, and
30 durations in each region. Detected swarms were considered candidates for shallow slow slip
31 events. A similar scaling relationship was observed between the cumulative moments and
32 activity areas, irrespective of regions. It indicates similar stress drops in each region. However,
33 the relationship between the cumulative moments and durations varied. This difference was
34 explained by the along-strike variations in the faulting conditions of shallow slow earthquakes,
35 such as material or hydrological properties.

36 **Plain Language Summary**

37 Slow earthquakes are characterized as slips much slower than similar-size regular earthquakes.
38 Although interactions between the shallow slow earthquakes and large tsunamigenic earthquakes
39 have often been discussed, our knowledge of the source characteristics and spatial variations of
40 the shallow slow earthquakes is still limited. In this study, we quantitatively investigated the
41 activity characteristics of shallow, very low frequency earthquakes (VLFEs) along the Nankai
42 Trough. Activity areas and released cumulative moments of shallow VLFE swarms exhibited a
43 similar scaling law irrespective of regions. However, the duration and cumulative moments of
44 the swarms varied in each region. These characteristics can provide key information on the
45 faulting conditions of slow earthquakes in shallow plate boundaries.

46 **1 Introduction**

47 Regular (fast) and slow earthquakes occur along plate boundaries in subduction zones to
48 release the accumulated stress due to subduction (summarized in Obara & Kato, 2016; Uchida &
49 Bürgmann, 2019). Different slip phenomena are separately distributed on the plate boundaries
50 (e.g., Dixon et al., 2014; Nishikawa et al., 2019; Takemura, Okuwaki, et al., 2020; Vaca et al.,
51 2018). These slips can be captured from geodetic and seismic observations. The total slips of
52 moderate-to-large earthquakes and small repeating earthquakes can be evaluated by geodetic
53 fault modeling (e.g., Hori et al., 2021; Okada, 1992) and empirical relationships between seismic
54 moments and slips (e.g., Nadeau & Johnson, 1998), respectively. However, it is still difficult to
55 evaluate small deformations due to slow slip events (SSEs), which are geodetic slips of slow
56 earthquakes with durations of several days to years. SSEs with Mw 5.5 and 6.5 are the detectable
57 limits in onshore and offshore regions, even when using dense Global Navigation Satellite
58 System observations in Japan (e.g., Agata et al., 2019; Nishimura et al., 2013; Suito, 2016).

59 Slow earthquakes can also be observed at seismic stations. Low frequency earthquakes
60 (LFEs) and tectonic tremors are observed in frequency ranges of 2-8 Hz (e.g., Obara, 2002).
61 Tremors can be considered superpositions of small LFEs (e.g., Shelly et al., 2007). Very low
62 frequency earthquakes (VLFEs) are observed in the lower frequency band (0.02–0.05 Hz) (e.g.,
63 Ghosh et al., 2015; Obara & Ito, 2005). When seismic slow earthquake swarms occur
64 simultaneously during SSEs, they are called episodic tremor and slip (ETS; Hirose & Obara,
65 2006; Rogers & Dragert, 2003). Small swarms of tremors and VLFEs without obvious geodetic
66 signals have often been observed around the world. Such small swarms can be considered

67 proxies of SSEs that have *Mw* smaller than the detectable limits of geodetic observations. Thus,
68 using dense onshore seismic networks, the characteristics of the swarms of deep LFEs and
69 tremors, which occur at deeper extensions of megathrust zones, have been investigated (e.g.,
70 Aiken & Obara, 2021; Daiku et al., 2018; Frank & Brodsky, 2019; Passarelli et al., 2021).
71 Empirical relationships between the geodetic moments of SSEs and seismic moments (or
72 energies) of swarms have been proposed for the monitoring of slips on plate boundaries.

73 Slow earthquakes occur at shallower extensions of megathrust zones in the offshore
74 regions of the Nankai subduction zone (Figure 1). Offshore observations revealed that
75 spatiotemporal correlation of various-type shallow slow earthquake phenomena (e.g., Araki et
76 al., 2017; Nakano et al., 2018; Yokota & Ishikawa, 2020). Because very low-frequency surface
77 waves from shallow VLFEs effectively propagate even in onshore regions and the offshore
78 observations are still limited, long-term activities of shallow VLFEs, especially in Nankai, have
79 been investigated from onshore broadband records (e.g., Baba et al., 2020; Takemura,
80 Matsuzawa, et al., 2019). From comparisons between their long-term catalogs and tectonic
81 environments, shallow VLFEs tend to be effectively activated by mechanical weakening due to
82 pore fluid pressure in the areas surrounding strongly locked zones.

83 To obtain more detailed characteristics of shallow VLFEs, Takemura et al. (2022)
84 conducted template matching and relocation for shallow VLFEs and evaluated their moment rate
85 functions southeast of the Kii Peninsula, Japan (Regions A and B in Figure 1). Due to their
86 techniques, estimations of epicenter locations and moment rate functions were improved from
87 the previous catalogs (Baba et al., 2020; Takemura, Matsuzawa, et al., 2019). From the spatial
88 distributions of the cumulative moments of shallow VLFEs, they confirmed a spatial relationship
89 between the cumulative moment of shallow VLFE and the paleo-Zenisu ridge, which subducted
90 southeast off the Kii Peninsula. In this study, we extend our previous work (Takemura et al.,
91 2022) to off the Cape Muroto and Kii Channel (Region C in Figure 1) to reveal along-strike
92 variations in shallow VLFE activity along the Nankai Trough. Then, we investigate the source
93 characteristics of shallow VLFE swarms, which are candidates for shallow SSEs, using our new
94 comprehensive moment-rate-function catalog of shallow VLFEs along the Nankai Trough. We
95 compare the cumulative moments of shallow VLFE swarms with the geodetic moments of the
96 corresponding shallow SSEs to discuss slip monitoring on the shallow plate boundary.
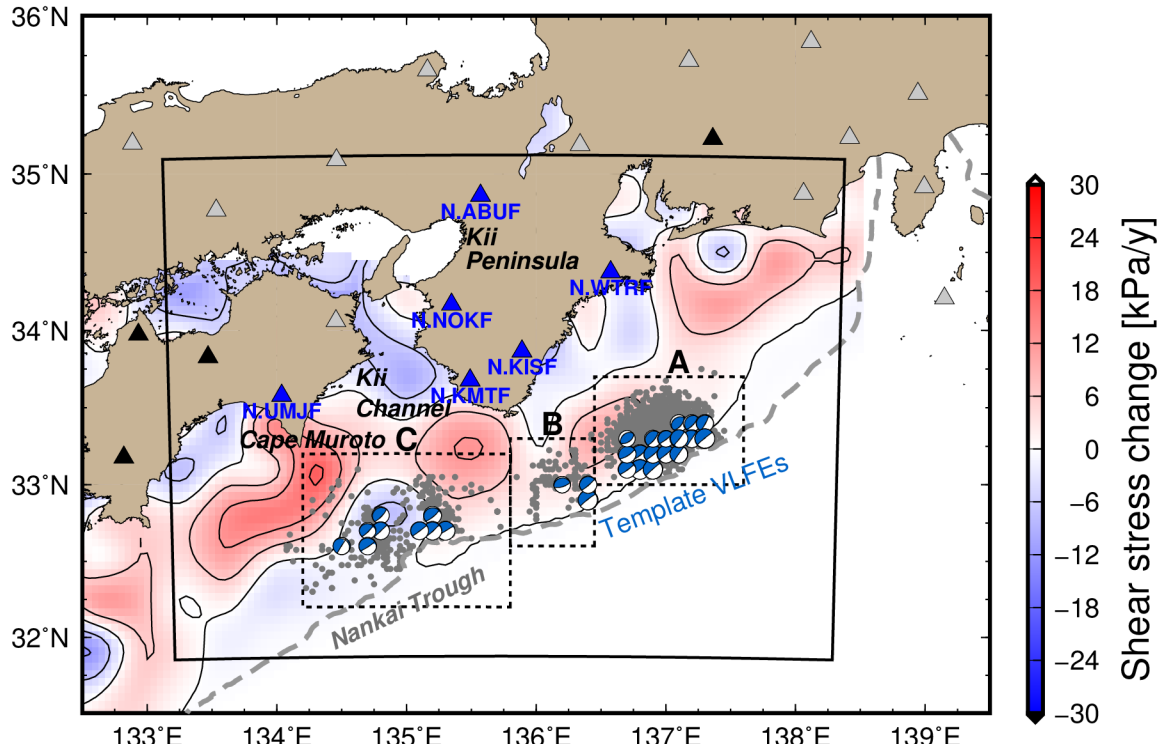
97

2 Data and Methods

99 We used broadband records from full-range seismograph network stations (F-net; Aoi et
100 al., 2020) that are operated by the National Research Institute for Earth Science and Disaster
101 Resilience (NIED), Japan. To avoid microseismic signals, we used a zero-phase Butterworth
102 filter with frequencies of 0.02–0.05 Hz. The analyzed period in this study ranged from April
103 2004 to March 2021. The detection and relocation processes of shallow VLFEs were similar to
104 those in Takemura, Noda, et al. (2019) (see Text S1 and Figure S1 of Takemura et al., 2022). We
105 conducted template matching analysis using template shallow VLFEs (blue focal spheres in
106 Figure 1). We divided the study area into three regions: (A) southeast of the Kii Peninsula, (B)
107 south of the Kii Peninsula, and (C) off the Cape Muroto and Kii Channel (dashed rectangles in
108 Figure 1).

109   After detection and relocation (gray circles in Figure 1), we estimated the moment rate
110   functions of the shallow VLFEs in Region C, which were constructed using a series of 6-s
111   Küpper wavelets. The weights of each Küpper pulse were estimated using a Monte-Carlo-based
112   simulated annealing method (Takemura et al., 2022). In our previous work (Takemura et al.,
113   2022), we already estimated moment rate functions of shallow VLFEs in Regions A and B. The
114   synthetic waveforms from sources with a single 6-s Küpper pulse were evaluated by reciprocal
115   calculations via OpenSWPC (Maeda et al., 2017) using the regional three-dimensional velocity
116   structure model (Koketsu et al., 2012; Takemura, Yabe, et al., 2020; Tonegawa et al., 2017).
117   Other technical details are provided in Text S1. An example of the estimated moment rate
118   function of the shallow VLFEs in Region C is illustrated in Figure S1. The fitness between the
119   observed and synthetic waveforms improved compared to those from the previous catalog
120   (Takemura, Matsuzawa, et al., 2019). We also compared the estimated moment rate function
121   with the velocity waveforms of the tremor band (2–8 Hz) at N.KMTF (Figure S2) and several
122   Hi-net stations (Figure S3). The envelope shapes of tremors typically correlate with the moment
123   rate functions of VLFEs (e.g., Ide et al., 2008; Yabe et al., 2019). Although high-frequency
124   seismograms can be complicated due to small-scale heterogeneities and subducting oceanic
125   plates (e.g., Furumura & Singh, 2002; Takemura et al., 2017), tremor envelopes also have multi-
126   peak packets. This supports the longer-duration and multi-peak moment rate functions of a
127   shallow VLFE. The shallow VLFEs with moment rates of approximately 5.0×10^{12} Nm/s is the
128   detectable lower limits (Figure 5b of Takemura et al., 2022).
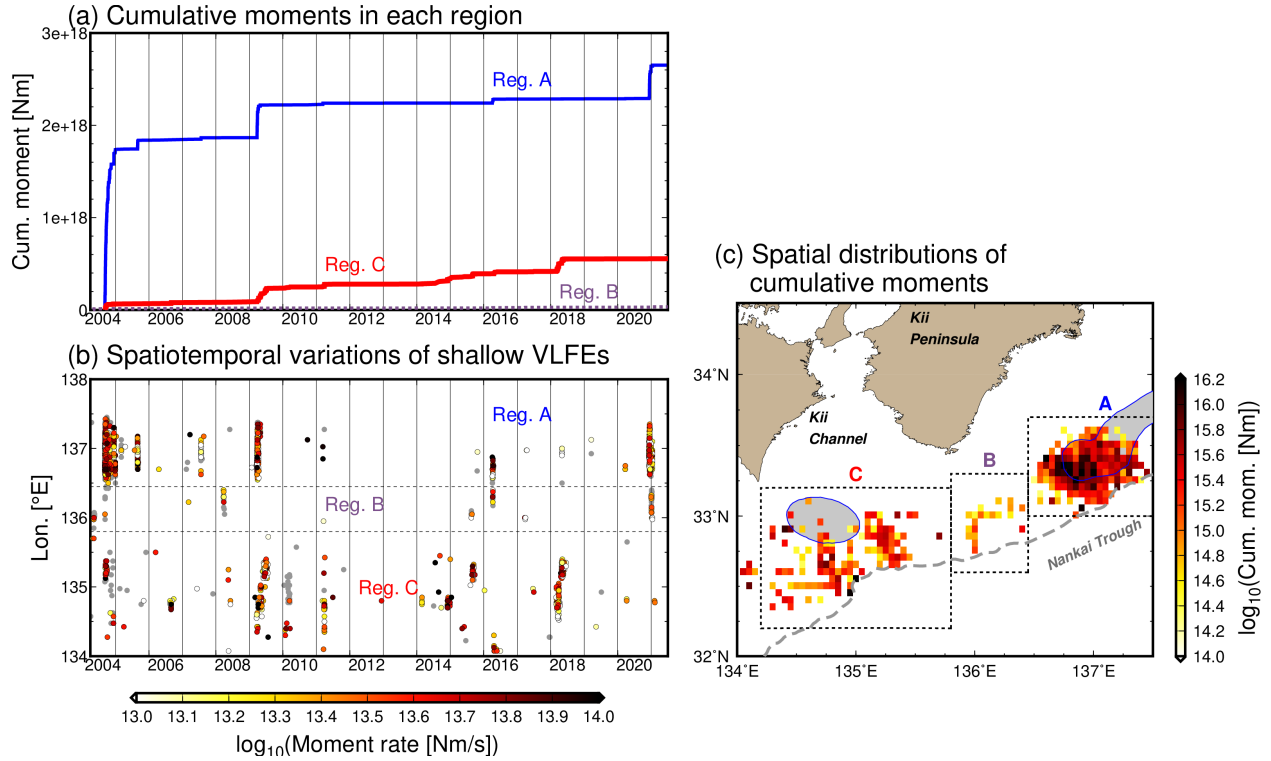
129   According to a comparison of size distributions between Takemura et al. (2022) and
130   Nakano et al. (2019), our catalog can stably include shallow VLFEs with $Mw \geq 3.7$.
131   Spatiotemporal distributions of shallow VLFE activity are illustrated in Figure 2. The cumulative
132   moment of shallow VLFEs at each region or grid was calculated by the sum of seismic moments
133   of shallow VLFEs with variance reductions (VRs) ≥ 30 % at a certain region or grid. Our new
134   catalog could catch larger cumulative moment releases than Takemura, Matsuzawa, et al. (2019),
135   due to template matching and our estimation method of moment rate function, but obtained
136   spatial variations are roughly similar as in previous studies (Takemura, Matsuzawa, et al., 2019).
137   The relationship between shallow VLFEs and tectonic environments, such as fluid and
138   seamounts, have also been discussed in other previous studies (e.g., Sun et al., 2020; Takemura
139   et al., 2022; Takemura, Matsuzawa, et al., 2019; Toh et al., 2020; Tonegawa et al., 2017). Then,
140   we focus our attention on characteristics of shallow VLFE swarms. After estimating the moment
141   rate function for shallow VLFEs in region C, we combined this catalog with our previous catalog
142   (Takemura et al., 2022; Regions A and B). From new catalog, we detected the shallow VLFE
143   swarms in each region based on the criteria proposed by Kurihara & Obara (2021). First, we
144   evaluated the expected inter-event times in each region by dividing the analysis period (17 y) by
145   the total number of shallow VLFEs in each region. In this study, shallow VLFE swarms were
146   defined as more than ten consequent shallow VLFEs with inter-event times shorter than the
147   expected inter-event time in each region. Examples of shallow VLFE swarms are presented in
148   Figure 2. The shallow VLFE episode from December 2020 was constructed by four shallow
149   VLFE swarms in regions A and B.

150   After swarm detection, we evaluated the cumulative moment, swarm duration, activity
151   areas, and along-strike spreading distance of each shallow VLFE swarm. The swarm durations
152   were calculated by the difference between the first and last events in each swarm. The swarm
153   duration of A-14 is illustrated in Figure 3a. The activity areas and along-strike spreading
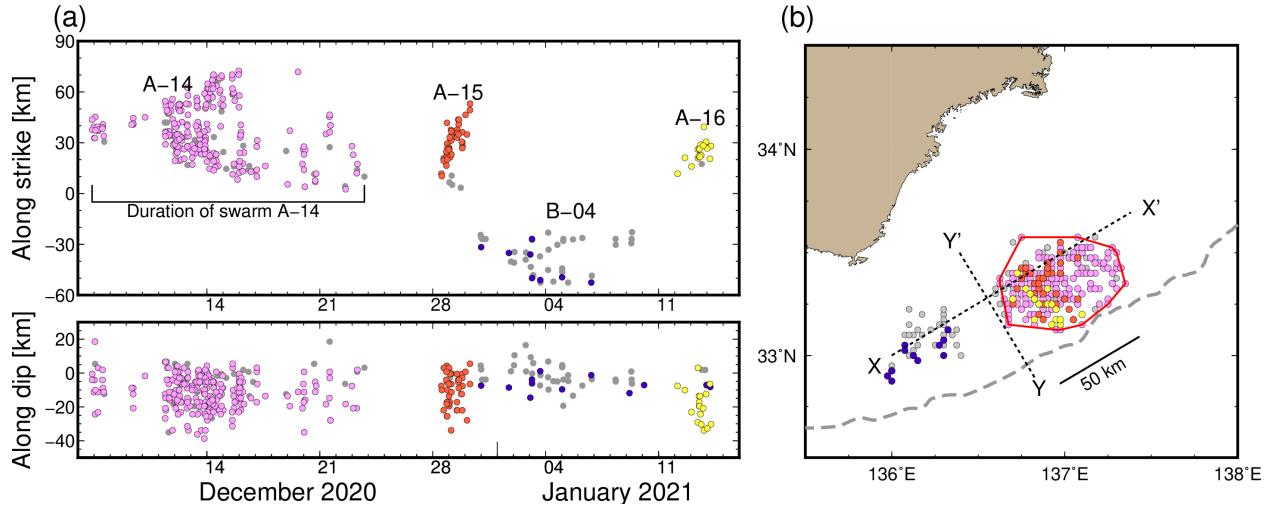
154 distances were calculated using the convex hull in the Python module (red enclosed area in
155 Figure 2b). To evaluate the cumulative moments and activity areas of the swarms, we used the
156 shallow VLFEs with VRs equal to or greater than 30%. The signals of shallow VLFEs with VRs
157 < 30 % tend to be weak compared to the noise signals. It should also be noted that because the
158 along-dip locations of shallow VLFEs have relatively large uncertainties due to station
159 distributions (see Figures 1b and 1d of Takemura, Noda, et al., 2019, and Figure S1 of Takemura
160 et al., 2022), their swarm areas are expected to be overestimated. The epicenter distributions in
161 the along-dip direction seem to be roughly two times larger than those estimated using ocean
162 bottom seismometers (Nakano et al., 2018).

163
164

Figure 1. Map of the Nankai region. Blue focal spheres are the template shallow VLFEs, which are well-constrained centroid moment tensor solutions derived from Takemura, Matsuzawa, et al. (2019). Gray circles are the epicenters of the detected shallow VLFEs. Shallow VLFEs in regions A and B are from Takemura et al. (2022). Shallow VLFEs in region C are from this study. Triangles denote the F-net stations. Stations with solid black and blue triangles were used for template matching and relocation. Stations represented by solid gray triangles were not used in the analysis. Moment rate function estimates for the detected VLFEs were derived from the data of the solid blue triangles. The black rectangle represents the horizontal calculation region for Green's functions. Background color in the map represents the shear stress change rate due to subduction of the Philippine Sea Plate (Noda et al., 2018). The gray dashed line represents the deformation front (Nankai Trough).

Figure 2. Spatiotemporal variations of 17 y of shallow VLFE data along the Nankai Trough. (a) Temporal variations of the cumulative moments of shallow VLFEs in each region. Blue solid, purple dotted, and red bold lines are cumulative moments of shallow VLFEs in regions A, B, and C, respectively. (b) Temporal variations of the along-strike shallow VLFE activity. The colors of each circle in (b) represent the moment rates of individual shallow VLFEs. Gray circles represent shallow VLFEs with VRs < 30%. (c) Spatial variation of cumulative moments from 17 y of shallow VLFE data. Spatial smoothing of the cumulative number and moments of shallow VLFEs were conducted within the region of 0.05° × 0.05° on the map via the gridding algorithm provided by Generic Mapping Tools (Wessel et al., 2013). The shaded areas represent the subducted seamounts around this region inferred from dense seismic surveys (Kodaira et al., 2000; Park et al., 2004).
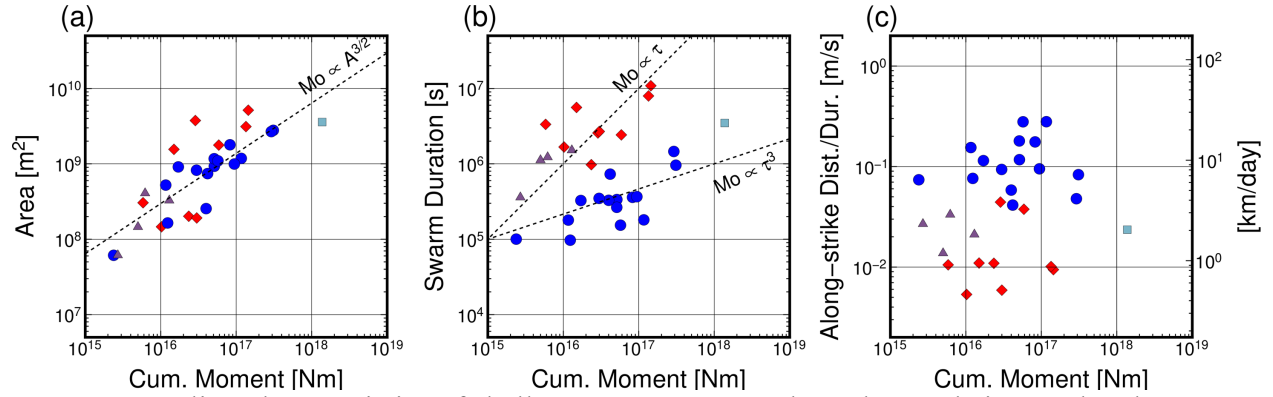
Figure 3. An example of shallow VLFE swarm detection. An example episode occurred in regions A and B from 6 December 2020 to 14 January 2021 (JST). Gray circles represent shallow VLFEs with VRs < 30%. (a) Temporal variations of shallow VLFE locations along-strike (X-X') and along-dip (Y-Y'). Colors represent swarm indices. (b) Map view of the shallow VLFE swarms from 6 December 2020 to 14 January 2021. The red enclosed area is the convex-hull of the swarm A-14. The intersection point between X-X' and Y-Y' in (b) represents X = 0 km and Y = 0 km in (a).

3 Results

We detected 16, 4, and 9 shallow VLFE swarms in regions A, B, and C, respectively (Table S1, Figure 4). The catalog of shallow VLFE including swarm index can be referred in Data Set S1. We discarded the A-01 swarm that started on September 6, 2004 (Figure S4) since this swarm might be triggered by the *Mw* 7.4 intraslab earthquake and aftershocks in region A (light blue square in Figure 4). Figure 4a shows the relationship between the cumulative moments and areas of the shallow VLFE swarms. Although along-dip locations of the relocated shallow VLFEs had relatively large uncertainties due to station distributions, the rupture area A approximately follows a scaling law similar to regular earthquakes and deep SSEs ($Mo \propto A^{3/2}$; Gao et al., 2012; Kanamori & Brodsky, 2004). A similar scaling law between the cumulative moments and areas irrespective of the regions indicates that stress drops of the shallow VLFE swarms should be similar in all regions. Regional differences were observed in the relationship between the cumulative moments and durations of the shallow VLFE swarms. The durations of the shallow VLFE swarms in region C were almost one order larger than those in region A. It was recently reported that LFEs, and LFE clusters likely follow $Mo \propto \tau^3$ rather than $Mo \propto \tau$ (e.g., Aiken & Obara, 2021; Supino et al., 2020). The durations of the shallow VLFE swarms in region A roughly followed $Mo \propto \tau^3$, rather than $Mo \propto \tau$. The $Mo \propto \tau$ is a typical scaling law of slow earthquake families (Ide et al., 2007). Such studies were difficult in regions B and C because of the insufficient number of shallow VLFE swarms.

Longer swarm durations in region C also indicate its slower spreading. Figure 4c shows the relationship between the cumulative moments and apparent spreading speeds, calculated by dividing the along-strike distances by each swarm duration. These speeds can be considered as the average along-strike rupture speeds of possible shallow SSEs. The apparent spreading speeds in region A range from 5 to 10 km/day, corresponding to the typical migration speeds of slow earthquakes (e.g., Houston et al., 2011; Obara, 2010). Several rapid (20–30 km/day, like A-15 in Figure 2) spreading have also been confirmed in this study. Shallow VLFE swarms in region C exhibit very slow (~1 km/day) spreading or cluster-like occurrences. The apparent spreading speeds in region B are intermediate between those of regions A and C.

Figure 4. Scaling characteristics of shallow VLFE swarms along the Nankai Trough. Blue circles, purple triangles, and red diamonds are the resultant values in regions A, B, and C, respectively. The light blue square represents the A-01 shallow VLFE swarm that started on September 6, 2004, which can be considered as a triggered VLFE swarm due to the *Mw* 7.4 intraslab earthquake. Cumulative moments versus (a) swarm activity areas, (b) swarm durations, and (c) apparent spreading speeds. The apparent spreading speed was evaluated by dividing the along-strike distance by the duration of each shallow VLFE swarm. Along-strike directions were 239º in regions A and B, and 245º in region C.

4. Discussion

        Spatiotemporal correlations between seismic and geodetic slow earthquakes have been found in deep slow earthquakes (e.g., Bartlow et al., 2011; Ito et al., 2007). During shallow SSE in April 2016, temporal increment in pore-fluid pressure at borehole observatory southeast off the Kii Peninsula well correlated temporal change in cumulative moments of corresponding shallow VLFEs (Nakano et al., 2018). Thus, the source characteristics of the shallow VLFE swarms can correlate with those of the background shallow SSEs. According to the relationship between cumulative moments and areas of shallow VLFE swarms (Figure 4a), the stress drops of shallow SSEs are expected to be similar irrespective of regions. However, the rupture velocities of shallow SSEs are different in the three regions (Figures 4b,c). This difference might be related to differences in the faulting conditions of each region (e.g., material properties). Pore fluid pressure may also be important. Laboratory experiments show that a small change in the ratio between the average fluid pressure and the average normal stress on the fault can induce a large change in rupture velocity (Passelègue et al., 2020). Tonegawa et al. (2017, 2022) suggested that pore fluid pressure around the plate boundary in region C is expected to be higher than that in region A. Observed differences in the migration velocity may also be caused by such fluid distribution.

        To obtain the broadband characteristics of shallow slow earthquakes along the Nankai Trough, we compared the cumulative moments of shallow VLFE swarms with those of corresponding shallow SSEs (Table S2). The cumulative moments of shallow VLFEs were approximately 2–18 % of those of the corresponding shallow SSEs. In this comparison, we also discarded shallow VLFEs with VRs < 30 %. We note that the effects of shallow VLFEs with VRs < 30 % on cumulative moment evaluation are limited. In contrast, the cumulative moment of deep VLFEs was only 0.1% of the corresponding deep SSEs (e.g., Ito et al., 2009). Passarelli et al. (2021) investigated the seismic productivities of slow earthquakes that were calculated by dividing the cumulative seismic moments of tremors (or earthquake swarms) by the geodetic moments of the corresponding SSEs. It was observed that seismic productivity decreases with increasing depth (Figures 2 and 4 in Passarelli et al., 2021). Daiku et al. (2018) demonstrated the relationship between the seismic productivities of deep ETSs and thermal structures at depths of 30–40 km in the Nankai Trough. Thus, we think that differences in seismic productivities between the shallow and deep VLFE swarms in the Nankai Trough may be correlated with depth differences in temperature, which control the frictional and rheological properties of the faults.

        A smaller number of shallow SSEs were reported (see Table S2) compared with the deep SSEs (see http://www-solid.eps.s.u-tokyo.ac.jp/~sloweq/; Kano et al., 2018). More shallow SSE fault models will allow us to analyze the quantitative relationship between them and VLFEs. In the future, the statistical characteristics of seismic productivity of shallow slow earthquakes in each region shall be obtained. Consequently, we will quantitatively monitor slips on the shallow plate boundary from seismic slow earthquakes (LFE, tremor, and VLFE).

5 Conclusions

285
286   Using continuous broadband records around the Nankai region, Japan, we revealed the
287 along-strike variations in shallow VLFE activity and source characteristics of shallow VLFE
288 swarms. Shallow VLFEs actively occur off the Cape Muroto, Kii Channel, and southeast off the
289 Kii Peninsula (regions A and C). These spatial variations of cumulative moments from shallow
290 VLFEs were updated and well agreed with the relationships with tectonic environments in
291 previous studies. Heterogeneous stress and structural properties due to the subducted seamounts
292 promote shallow slow earthquakes along the Nankai Trough.

293   We investigated the shallow VLFE swarms in each region, which could be candidates for
294 shallow SSEs. We conclude that the cumulative moments and activity areas of shallow VLFE
295 swarms follow a similar scaling law irrespective of region, indicated by similar stress drop
296 values. However, relationships between the cumulative moments and durations of the shallow
297 VLFE swarms vary in each region. The apparent spreading speeds are also variable
298 characteristics. These differences can be explained by regional differences in the faulting
299 conditions of the shallow slow earthquakes, such as material or hydrological properties.

Data availability statement

311
312 The Python package HinetPy (Tian, 2020) was used to download the NIED F-net/Hi-net
313 continuous records (National Research Institute for Earth Science and Disaster Resilience,
314 2019a, 2019b). We simulated the Green's functions in the local 3D model using OpenSWPC
315 version 5.1.0 https://doi.org/10.5281/zenodo.3982232. The modified 1D layered velocity models
316 of Tonegawa et al. (2017) can be downloaded from https://doi.org/10.5281/zenodo.4158947. The
317 model of Koketsu et al. (2012) was obtained from
318 https://www.jishin.go.jp/evaluation/seismic_hazard_map/lpshm/12_choshuki_dat/. We used the
319 seismic analysis code (Goldstein & Snoke, 2005; Helffrich et al., 2013) and generic mapping tools
320 (Wessel et al., 2013) for signal processing and figure drawing. Data analysis was conducted
321 using NumPy (Harris et al., 2020), SciPy 1.7.0 (https://doi.org/10.5281/zenodo.5000479), and
322 Pandas 1.2.5 (https://doi.org/10.5281/zenodo.5013202). The estimated moment rate functions of
323 shallow VLFEs along the Nankai Trough can be downloaded from
324 https://doi.org/10.5281/zenodo.5211090 and https://doi.org/10.5281/zenodo.5824418.
325

References

Agata, R., Hori, T., Ariyoshi, K., & Ichimura, T. (2019). Detectability analysis of interplate fault slips in the Nankai subduction thrust using seafloor observation instruments. *Marine Geophysical Research*. https://doi.org/10.1007/s11001-019-09380-y

Aiken, C., & Obara, K. (2021). Data-Driven Clustering Reveals More Than 900 Small Magnitude Slow Earthquakes and Their Characteristics. *Geophysical Research Letters*, *48*(11). https://doi.org/10.1029/2020GL091764

Aoi, S., Asano, Y., Kunugi, T., Kimura, T., Uehira, K., Takahashi, N., et al. (2020). MOWLAS: NIED observation network for earthquake, tsunami and volcano. *Earth, Planets and Space*, *72*(1). https://doi.org/10.1186/s40623-020-01250-x

Araki, E., Saffer, D. M., Kopf, A. J., Wallace, L. M., Kimura, T., Machida, Y., et al. (2017). Recurring and triggered slow-slip events near the trench at the Nankai Trough subduction megathrust. *Science*, *356*(6343), 1157–1160. https://doi.org/10.1126/science.aan3120

Baba, S., Takemura, S., Obara, K., & Noda, A. (2020). Slow earthquakes illuminating interplate coupling heterogeneities in subduction zones. *Geophysical Research Letters*, 4–5. https://doi.org/10.1029/2020gl088089

Bartlow, N. M., Miyazaki, S., Bradley, A. M., & Segall, P. (2011). Space-time correlation of slip and tremor during the 2009 Cascadia slow slip event. *Geophysical Research Letters*, *38*(18), 1–6. https://doi.org/10.1029/2011GL048714

Daiku, K., Hiramatsu, Y., Matsuzawa, T., & Mizukami, T. (2018). Slow slip rate and excitation efficiency of deep low-frequency tremors beneath southwest Japan. *Tectonophysics*, *722*(May 2017), 314–323. https://doi.org/10.1016/j.tecto.2017.11.016

Dixon, T. H., Jiang, Y., Malservisi, R., McCaffrey, R., Voss, N., Protti, M., & Gonzalez, V. (2014). Earthquake and tsunami forecasts: Relation of slow slip events to subsequent earthquake rupture. *Proceedings of the National Academy of Sciences*, *111*(48), 17039–17044. https://doi.org/10.1073/pnas.1412299111

Frank, W. B., & Brodsky, E. E. (2019). Daily measurement of slow slip from low-frequency earthquakes is consistent with ordinary earthquake scaling, (October), 1–7.

Furumura, T., & Singh, S. K. (2002). Regional wave propagation from Mexican subduction zone earthquakes: The attenuation functions for interplate and inslab events. *Bulletin of the Seismological Society of America*, *92*(6), 2110–2125. https://doi.org/10.1785/0120010278

Gao, H., Schmidt, D. A., & Weldon, R. J. (2012). Scaling Relationships of Source Parameters for Slow Slip Events. *Bulletin of the Seismological Society of America*, *102*(1), 352–360. https://doi.org/10.1785/0120110096

Ghosh, A., Huesca-Pérez, E., Brodsky, E., & Ito, Y. (2015). Very low frequency earthquakes in Cascadia migrate with tremor. *Geophysical Research Letters*, *42*(9), 3228–3232. https://doi.org/10.1002/2015GL063286

Goldstein, P., & Snoke, A. (2005). SAC Availability for the IRIS Community. Retrieved from https://ds.iris.edu/ds/newsletter/vol7/no1/193/sac-availability-for-the-iris-community/

Harris, C. R., Millman, K. J., van der Walt, S. J., Gommers, R., Virtanen, P., Cournapeau, D., et al. (2020). Array programming with NumPy. *Nature*, *585*(7825), 357–362. https://doi.org/10.1038/s41586-020-2649-2

Helffrich, G., Wookey, J., & Bastow, I. (2013). *The Seismic Analysis Code*. Cambridge: Cambridge University Press. https://doi.org/10.1017/CBO9781139547260

Hirose, H., & Obara, K. (2006). Short-term slow slip and correlated tremor episodes in the Tokai region, central Japan. *Geophysical Research Letters*, *33*(17), L17311. https://doi.org/10.1029/2006GL026579

Hori, T., Agata, R., Ichimura, T., Fujita, K., Yamaguchi, T., & Iinuma, T. (2021). High-fidelity elastic Green's functions for subduction zone models consistent with the global standard geodetic reference system. *Earth, Planets and Space*, *73*(1). https://doi.org/10.1186/s40623-021-01370-y

Houston, H., Delbridge, B. G., Wech, A. G., & Creager, K. C. (2011). Rapid tremor reversals in Cascadia generated by a weakened plate interface. *Nature Geoscience*, *4*(6), 404–409. https://doi.org/10.1038/ngeo1157

Ide, S., Beroza, G. C., Shelly, D. R., & Uchide, T. (2007). A scaling law for slow earthquakes. *Nature*, *447*(7140), 76–79. https://doi.org/10.1038/nature05780

Ide, S., Imanishi, K., Yoshida, Y., Beroza, G. C., & Shelly, D. R. (2008). Bridging the gap between seismically and geodetically detected slow earthquakes. *Geophysical Research Letters*, *35*(10), 2–7. https://doi.org/10.1029/2008GL034014

Ito, Y., Obara, K., Shiomi, K., Sekine, S., & Hirose, H. (2007). Slow earthquakes coincident with episodic tremors and slow slip events. *Science*, *315*(5811), 503–506. https://doi.org/10.1126/science.1134454

379 Ito, Y., Obara, K., Matsuzawa, T., & Maeda, T. (2009). Very low frequency earthquakes related to small asperities
380   on the plate boundary interface at the locked to aseismic transition. *Journal of Geophysical Research: Solid*
381   *Earth*, *114*(B11), 1–16. https://doi.org/10.1029/2008JB006036
382 Kanamori, H., & Brodsky, E. E. (2004). The physics of earthquakes. *Reports on Progress in Physics*, *67*(8), 1429–
383   1496. https://doi.org/10.1088/0034-4885/67/8/R03
384 Kano, M., Aso, N., Matsuzawa, T., Ide, S., Annoura, S., Arai, R., et al. (2018). Development of a slow earthquake
385   database. *Seismological Research Letters*, *89*(4), 1566–1575. https://doi.org/10.1785/0220180021
386 Kodaira, S., Takahashi, N., Nakanishi, A., Miura, S., & Kaneda, Y. (2000). Subducted seamount imaged in the
387   rupture zone of the 1946 Nankaido earthquake. *Science*, *289*(5476), 104–106.
388   https://doi.org/10.1126/science.289.5476.104
389 Koketsu, K., Miyake, H., & Suzuki, H. (2012). Japan Integrated Velocity Structure Model Version 1. *Proceedings of*
390   *the 15th World Conference on Earthquake Engineering*, 1–4. Retrieved from
391   http://www.iitk.ac.in/nicee/wcee/article/WCEE2012_1773.pdf
392 Kurihara, R., & Obara, K. (2021). Spatiotemporal Characteristics of Relocated Deep Low-Frequency Earthquakes
393   Beneath 52 Volcanic Regions in Japan Over an Analysis Period of 14 Years and 9 Months. *Journal of*
394   *Geophysical Research: Solid Earth*, *126*(10). https://doi.org/10.1029/2021JB022173
395 Maeda, T., Takemura, S., & Furumura, T. (2017). OpenSWPC : An open-source integrated parallel simulation code
396   for mod- eling seismic wave propagation in 3D heterogeneous viscoelastic media.
397 Nadeau, R. M., & Johnson, J. R. (1998). Seismological Studies at Parkfield IV: Moment Releaase Rates and
398   Estimates of Source Parameters for Small Repeating Earthquakes. *Bull. Seis. Soc. Am.*, *88*(3), 790–814.
399 Nakano, M., Hori, T., Araki, E., Kodaira, S., & Ide, S. (2018). Shallow very-low-frequency earthquakes accompany
400   slow slip events in the Nankai subduction zone. *Nature Communications*, *9*(1), 984.
401   https://doi.org/10.1038/s41467-018-03431-5
402 Nakano, M., Yabe, S., Sugioka, H., Shinohara, M., & Ide, S. (2019). Event Size Distribution of Shallow Tectonic
403   Tremor in the Nankai Trough. *Geophysical Research Letters*, *46*(11), 5828–5836.
404   https://doi.org/10.1029/2019GL083029
405 National Research Institute for Earth Science and Disaster Resilience. (2019a). NIED F-net.
406   https://doi.org/10.17598/NIED.0005
407 National Research Institute for Earth Science and Disaster Resilience. (2019b). NIED Hi-net.
408   https://doi.org/10.17598/NIED.0003
409 Nishikawa, T., Matsuzawa, T., Ohta, K., Uchida, N., Nishimura, T., & Ide, S. (2019). The slow earthquake spectrum
410   in the Japan Trench illuminated by the S-net seafloor observatories. *Science*, *365*(August), 808–813.
411   https://doi.org/10.1126/science.aax5618
412 Nishimura, T., Matsuzawa, T., & Obara, K. (2013). Detection of short-term slow slip events along the Nankai
413   Trough, southwest Japan, using GNSS data. *Journal of Geophysical Research: Solid Earth*, *118*(6), 3112–
414   3125. https://doi.org/10.1002/jgrb.50222
415 Noda, A., Saito, T., & Fukuyama, E. (2018). Slip-Deficit Rate Distribution Along the Nankai Trough, Southwest
416   Japan, With Elastic Lithosphere and Viscoelastic Asthenosphere. *Journal of Geophysical Research: Solid*
417   *Earth*, *123*(9), 8125–8142. https://doi.org/10.1029/2018JB015515
418 Obara, K. (2002). Nonvolcanic deep tremor associated with subduction in southwest Japan. *Science*, *296*(5573),
419   1679–1681. https://doi.org/10.1126/science.1070378
420 Obara, K. (2010). Phenomenology of deep slow earthquake family in southwest Japan: Spatiotemporal
421   characteristics and segmentation. *Journal of Geophysical Research: Solid Earth*, *115*(8), 1–22.
422   https://doi.org/10.1029/2008JB006048
423 Obara, K., & Ito, Y. (2005). Very low frequency earthquakes excited by the 2004 off Kii peninsula earthquakes: A
424   dynamic deformation process in the large accretionary prism. *Earth, Planets and Space*, *57*(4), 321–326.
425   https://doi.org/10.1186/BF03352570
426 Obara, K., & Kato, A. (2016). Connecting slow earthquakes to huge earthquakes. *Science*, *353*(6296), 253–257.
427   https://doi.org/10.1126/science.aaf1512
428 Okada, Y. (1992). Internal Deformation due to Shear and Tensile Faults in a Half-space. *Bulletin of the*
429   *Seismological Society of America*, *82*(2), 1018–1040.
430 Park, J.-O., Moore, G. F., Tsuru, T., Kodaira, S., & Kaneda, Y. (2004). A subducted oceanic ridge influencing the
431   Nankai megathrust earthquake rupture. *Earth and Planetary Science Letters*, *217*(1–2), 77–84.
432   https://doi.org/10.1016/S0012-821X(03)00553-3
433 Passarelli, L., Selvadurai, P. A., Rivalta, E., & Jónsson, S. (2021). The source scaling and seismic productivity of
434   slow slip transients. *Science Advances*, *7*(32). https://doi.org/10.1126/sciadv.abg9718

Passelègue, F. X., Almakari, M., Dublanchet, P., Barras, F., Fortin, J., & Violay, M. (2020). Initial effective stress controls the nature of earthquakes. *Nature Communications*, *11*(1), 1–8. https://doi.org/10.1038/s41467-020-18937-0

Rogers, G., & Dragert, H. (2003). Episodic tremor and slip on the Cascadia subduction zone: the chatter of silent slip. *Science*, *300*(5627), 1942–1943. https://doi.org/10.1126/science.1084783

Shelly, D. R., Beroza, G. C., & Ide, S. (2007). Non-volcanic tremor and low-frequency earthquake swarms. *Nature*, *446*(7133), 305–307. https://doi.org/10.1038/nature05666

Suito, H. (2016). Detectability of Interplate Fault Slip around Japan, Based on GEONET Daily Solution F3 (in Japanese with English abstract). *Journal of the Geodetic Society of Japan*, *62*(3), 109–120. https://doi.org/10.11366/sokuchi.62.109

Sun, T., Saffer, D., & Ellis, S. (2020). Mechanical and hydrological effects of seamount subduction on megathrust stress and slip. *Nature Geoscience*, *13*(March). https://doi.org/10.1038/s41561-020-0542-0

Supino, M., Poiata, N., Festa, G., Vilotte, J. P., Satriano, C., & Obara, K. (2020). Self-similarity of low-frequency earthquakes. *Scientific Reports*, *10*(1), 1–9. https://doi.org/10.1038/s41598-020-63584-6

Takemura, S., Kobayashi, M., & Yoshimoto, K. (2017). High-frequency seismic wave propagation within the heterogeneous crust: effects of seismic scattering and intrinsic attenuation on ground motion modelling. *Geophysical Journal International*, *210*(3), 1806–1822. https://doi.org/10.1093/gji/ggx269

Takemura, S., Noda, A., Kubota, T., Asano, Y., Matsuzawa, T., & Shiomi, K. (2019). Migrations and Clusters of Shallow Very Low Frequency Earthquakes in the Regions Surrounding Shear Stress Accumulation Peaks Along the Nankai Trough. *Geophysical Research Letters*, *46*(21), 11830–11840. https://doi.org/10.1029/2019GL084666

Takemura, S., Matsuzawa, T., Noda, A., Tonegawa, T., Asano, Y., Kimura, T., & Shiomi, K. (2019). Structural Characteristics of the Nankai Trough Shallow Plate Boundary Inferred From Shallow Very Low Frequency Earthquakes. *Geophysical Research Letters*, *46*(8), 4192–4201. https://doi.org/10.1029/2019GL082448

Takemura, S., Okuwaki, R., Kubota, T., Shiomi, K., Kimura, T., & Noda, A. (2020). Centroid moment tensor inversions of offshore earthquakes using a three-dimensional velocity structure model: slip distributions on the plate boundary along the Nankai Trough. *Geophysical Journal International*, *222*(2), 1109–1125. https://doi.org/10.1093/gji/ggaa238

Takemura, S., Yabe, S., & Emoto, K. (2020). Modelling high-frequency seismograms at ocean bottom seismometers: effects of heterogeneous structures on source parameter estimation for small offshore earthquakes and shallow low-frequency tremors. *Geophysical Journal International*, *223*(3), 1708–1723. https://doi.org/10.1093/gji/ggaa404

Takemura, S., Obara, K., Shiomi, K., & Baba, S. (2022). Spatiotemporal Variations of Shallow Very Low Frequency Earthquake Activity Southeast Off the Kii Peninsula, Along the Nankai Trough, Japan. *Journal of Geophysical Research: Solid Earth*, *127*(3), e2021JB023073. https://doi.org/10.1029/2021JB023073

Tian, D. (2020). HinetPy: A Python package to request and process seismic waveform data from Hi-net. https://doi.org/10.5281/zenodo.3885779

Toh, A., Chen, W. J., Takeuchi, N., Dreger, D. S., Chi, W. C., & Ide, S. (2020). Influence of a Subducted Oceanic Ridge on the Distribution of Shallow VLFEs in the Nankai Trough as Revealed by Moment Tensor Inversion and Cluster Analysis. *Geophysical Research Letters*, *47*(15), 0–3. https://doi.org/10.1029/2020GL087244

Tonegawa, T., Araki, E., Kimura, T., Nakamura, T., Nakano, M., & Suzuki, K. (2017). Sporadic low-velocity volumes spatially correlate with shallow very low frequency earthquake clusters. *Nature Communications*, *8*(1), 2048. https://doi.org/10.1038/s41467-017-02276-8

Tonegawa, T., Takemura, S., Yabe, S., & Yomogida, K. (2022). Fluid migration before and during slow earthquakes in the shallow Nankai subduction zone. *Journal of Geophysical Research: Solid Earth*. https://doi.org/10.1029/2021JB023583

Uchida, N., & Bürgmann, R. (2019). Repeating Earthquakes. *Annual Review of Earth and Planetary Sciences*, *47*(1), 305–332. https://doi.org/10.1146/annurev-earth-053018-060119

Vaca, S., Vallée, M., Nocquet, J. M., Battaglia, J., & Régnier, M. (2018). Recurrent slow slip events as a barrier to the northward rupture propagation of the 2016 Pedernales earthquake (Central Ecuador). *Tectonophysics*, *724–725*(November 2017), 80–92. https://doi.org/10.1016/j.tecto.2017.12.012

Wessel, P., Smith, W. H. F., Scharroo, R., Luis, J., & Wobbe, F. (2013). Generic mapping tools: Improved version released. *Eos*, *94*(45), 409–410. https://doi.org/10.1002/2013EO450001

Yabe, S., Tonegawa, T., & Nakano, M. (2019). Scaled Energy Estimation for Shallow Slow Earthquakes. *Journal of Geophysical Research: Solid Earth*, *124*(2), 1507–1519. https://doi.org/10.1029/2018JB016815

490   Yokota, Y., & Ishikawa, T. (2020). Shallow slow slip events along the Nankai Trough detected by GNSS-A. *Science*
491   *Advances*, *6*(3), eaay5786. https://doi.org/10.1126/sciadv.aay5786
492
493